The Astronomical Journal, 151:149 (13pp), 2016 June doi:10.3847/0004-6256/151/6/149

GR 290 (ROMANO'S STAR). II. LIGHT HISTORY AND EVOLUTIONARY STATE

V. F. Polcaro[1], O. Maryeva[2], R. Nesci[1], M. Calabresi[3], A. Chieffi[1], S. Galleti[4], R. Gualandi[4], R. Haver[3], O. F. Mills[5], W. H. Osborn[5], A. Pasquali[6], C. Rossi[7], T. Vasilyeva[8], and R. F. Viotti[1]
[1] INAF-IAPS, Via del Fosso del Cavaliere, 100, I-00133 Roma, Italy; vitofrancesco.polcaro@iaps.inaf.it
[2] Special Astrophysical Observatory of the Russian Academy of Science, Nizhnii Arkhyz, 369167, Russia
[3] ARA, Via Carlo Emanuele I, 12A, I-00185 Roma, Italy
[4] INAF—Osservatorio Astronomico di Bologna, Via Ranzani 1, I-40127 Bologna, Italy
[5] Yerkes Observatory, 373 W. Geneva Street, Williams Bay, WI 53115, USA
[6] Astronomisches Rechen-Institut, Zentrum für Astronomie, Universität Heidelberg, Mönchhofstrasse 12-14, D-69120 Heidelberg, Germany
[7] Università La Sapienza, Pza A.Moro 5, I-00185 Roma, Italy
[8] Pulkovo Astronomical Observatory, 196140, Saint-Petersburg, Pulkovskoye chaussee 65/1, Russia
Received 2016 February 2; accepted 2016 March 14; published 2016 May 25

ABSTRACT

We have investigated the past light history of the luminous variable star GR 290 (M33/V532, Romano's Star) in the M33 galaxy, and collected new spectrophotometric observations in order to analyze links between this object, the LBV category, and the Wolf–Rayet stars of the nitrogen sequence. We have built the historical light curve of GR 290 back to 1901, from old observations of the star found in several archival plates of M33. These old recordings together with published and new data on the star allowed us to infer that for at least half a century the star was in a low luminosity state, with $B \simeq 18$–19, most likely without brighter luminosity phases. After 1960, five large variability cycles of visual luminosity were recorded. The amplitude of the oscillations was seen increasing toward the 1992–1994 maximum, then decreasing during the last maxima. The recent light curve indicates that the photometric variations have been quite similar in all the bands and that the $B-V$ color index has been constant within $\pm 0.1^m$ despite the 1.5^m change of the visual luminosity. The spectrum of GR 290 at the large maximum of 1992–94 was equivalent to late-B-type, while, during 2002–2014, it varied between WN10h-11h near the visual maxima to WN8h-9h at the luminosity minima. We have detected, during this same period, a clear anti-correlation between the visual luminosity, the strength of the He II 4686 Å emission line, the strength of the 4600–4700 Å lines' blend, and the spectral type. From a model analysis of the spectra collected during the whole 2002–2014 period, we find that the Rosseland radius $R_{2/3}$, changed between the minimum and maximum luminosity phases by a factor of three while $T_{\rm eff}$ varied between about 33,000 and 23,000 K. We confirm that the bolometric luminosity of the star has not been constant, but has increased by a factor of ∼1.5 between minimum and maximum luminosity, in phase with the apparent luminosity variations. Presently, GR 290 falls in the H–R diagram close to WN8h stars and is probably younger than them. In the light of current evolutionary models of very massive stars, we find that GR 290 has evolved from an ∼60 $M_\odot$ progenitor star and should have an age of about four million years. From its physical charcteristics, we argue that GR 290 has left the LBV stage and is presently moving from the LBV stage to a Wolf–Rayet stage of a late nitrogen spectral type.

Key words: galaxies: individual (M33) – stars: evolution – stars: individual (GR 290, M33 V0532) – stars: variables: general – stars: Wolf–Rayet

1. INTRODUCTION

GR 290, also known as Romano's star or M33/V532, in the M33 galaxy was discovered as a variable star in 1978 by Romano (1978a), who later described its ample variation as similar to that of Hubble–Sandage variables (Romano 1978b).

Extensive studies of GR 290 were performed in recent years (see, for example, Polcaro et al. (2011), hereafter Paper 1; Sholukhova et al. (2011); Clark et al. (2012) and references therein). In Paper 1, we investigated the spectral and photometric variations of GR 290 during the 2003–2010 period and have underlined many important features of the star, namely, the spectral type being constantly hotter than for other LBV, and the anti-correlation between the visual luminosity and the excitation of the emission lines. In spite of the many studies on GR 290, several questions remain unresolved, for example, the light curve that has been measured so far seems peculiar with respect to the photometrically studied LBVs. Furthermore, the hot spectrum of GR 290 is unusual for an LBV and may be an indication of the star leaving (or having already left) the LBV stage (see Paper 1; Humphreys et al. 2014). Recently, a new light minimum, still ongoing at the time of writing, has been reported by Calabresi et al. (2014). This has stimulated us to investigate the nature of this star in more depth.

The aim of this paper is to use the light and spectral variations to trace the past evolution of GR 290, define its present stage, and possibly predict its future behavior. Following the Introduction, Section 2 tackles the historical and recent light curve. Section 3 is devoted to the spectral variations of the star, and Section 4 discusses its evolutionary phase.

2. THE LIGHT CURVE

The earliest, targetted observations of GR 290, as performed by Romano (1978b), covered the period of 1960–1977. New observations for the period of 1982–1999 were published by Kurtev et al. (2001), while a very extended list of observations collected at the Crimea Observatory (since 1961) and the Special Astrophysical Observatory (SAO, since 2001) were reported by Sholukhova et al. (2011). These observations,

together with those published in Paper 1, allow us to analyze only the recent "active phase" of the star. Since nothing is known about the behavior of GR 290 before 1960, we have searched for available old plates of the M33 galaxy containing our target.

2.1. Historical Plates

We have found many digitized images of historical plates obtained by several observatories before 1940. Nine useful plates of M33 can be found in the Hamburg Observatory archive, taken with the 1 m $F/3$ Newtonian telescope. The digitized images are available online in fits format.[9] We have also found a good number of useful plates taken with the 72 cm $F/3.9$ reflector between 1907 and 1922 in the Heidelberg online archive.[10] Other plates, found in the Pulkovo Photographic Plate Database[11] (Kiseleva & Khrutskaya 2007), were obtained between 1935 and 1938 with the the 33 cm $F/11$ Normal astrograph of the observatory.

Several plates have also been found in the Yerkes Observatory plate archive, most of them obtained with the Yerkes old 24 inch (60 cm) $F/3.87$ reflector, exposed between 1901 and 1952. Further historic photometric points could be obtained from the POSS plates available online and from some Asiago plates not used by G. Romano in his original paper.

The blue plate of the POSS-I survey is not available online, thus we only measured the red plate: GR 290 in this plate is rather faint, outside the range of our photometric sequence, so its magnitude is extrapolated and must be considered rather uncertain. In this case, we included in the comparison sequence the star M31a-314 ($R = 17.83$) to extend the calibration range. In all Hamburg plates, GR 290 is clearly visible except in S02396, though it is generally close to the plate magnitude limit. The bright flux measured in the S02436 plate is uncertain due to the strong coma and the noisy appearance of the emulsion: it would indicate a variation of half magnitude in three months, however, which is not unusual for this source as also shown below. In several Heidelberg and Yerkes plates, the star is not visible, hence only upper limits could be derived. In all of the plates, the star was substantially fainter than the values reported by Romano (1978b) for the years 1960–62, but is consistent with the magnitude measured during the recent minima.

All of the technical details concerning the data reduction of the archival images are reported in the Appendix. Table 1 lists all of the archival magnitudes as derived from our photometric procedure.

All of the old photometric observations are reported in the upper panel of Figure 1, where we also give the more recent B-filter observations. Some upper limits, which better define the star light curve, have also been shown.

2.2. New Photometry

Since 2010 December, new photometric observations in the B, V, and R bands were collected in Italy with the 1.52 m Cassini telescope at the Loiano Station of the Bologna Astronomical Observatory-INAF, with the 37 cm telescope of Frasso Sabino of the Associazione Romana Astrofili (ARA), and with the 30 cm telescope of Franco Montagni at Greve. We also observed GR 290 with the 80 cm Tenerife telescope of the Instituto Astrofisico de Canarias (IAC) in 2012 October and 2013 October. We also made use of data collected with the 61 cm robotic telescope of the Sierra Stars Observatory Network in Mount Lemmon (Arizona). Table 2 reports our new photometric observations, including two U-band values recorded at the Loiano Observatory on 2015 November 14 and December 11. These new B, V, R observations collected since 2010 are shown, together with the old ones, in the lower panel of Figure 1.

2.3. Discussion of the Light Curve of GR 290

As can be seen in Figure 1, the historical light curve of GR 290 covers a period of more than one century, including a long period of low apparent brightness at $17.5 < B < 18.5$ (± 0.2 mag) during the first half of the twentieth century (*quiescent phase*), followed by a sequence of transitions between low and high visual luminosity (*active phase*). According to Figure 1, one can identify at least five broad light maxima (before 1974, 1983, 1992–94, 2004, and 2010) that have occurred since 1960 and five light minima (in 1975–79, 1983–86, 2000–2002, 2007–2009, and 2013 to present). In particular, the recorded maxima are characterized by different peak luminosities: the first three maxima increased their peak luminosity, which culminated with the 1992–94 maximum, while the last two occurred with a decreasing peak luminosity. Also the last three light minima were of decreasing luminosity. Hence, the photometric trend following the largest 1992–94 maximum might suggest that the star is gradually recovering a new stationary state through a sequence of oscillations with decreasing apparent brightness. As discussed below, this trend is also marked by the spectroscopic variations of the star. In addition, the light curve shows irregular photometric variations on timescales of weeks to months. For instance, one can see in the lower panel of Figure 1, that, between 1994 October and 1995 December, GR 290 was subject to a short event during which its luminosity dropped by at least one magnitude with fairly rapid luminosity decrease and increase. No light oscillation of such amplitude has been detected in the recent light curve.

It is generally observed that, during the S Dor phase, the color of LBVs is bluer at the light minimum than near the light maximum. In Paper 1, we show that the light curves in the B, V, and R bands nearly overlap without a clear luminosity variation (see also Figure 1 in Paper 1). Having now at our disposal a conspicuous amount of multicolor photometric observations covering an ample time interval, we have plotted in Figure 2 the $(B - V)$ color index versus visual magnitude between 2003 February and 2014 December.

The variations in $(B - V)$ are well within the error bars, with a mean value of about -0.06 mag and there is no clear evidence for a variation of $(B - V)$ as a function of the visual magnitude. The different behavior of the $(B - V)$ color with the stellar magnitude given by Sholukhova et al. (2011) has to be attributed to the larger uncertainty of their photometry. We conclude that, within the errors, the $(B - V)$ color index of GR 290 has basically been constant during recent cycles, suggesting that the blue-visual slope of the spectrum has remained substantially unchanged in spite of the ample spectral and brightness variation. This behavior, which is different from what is generally expected for the S Dor variations of LBVs, can be attributed to the continuum opacity, which, at the high

[9] http://plate-archive.hs.uni-hamburg.de/index.php/en/
[10] http://dc.zah.uni-heidelberg.de/lswscans/res/positions/fullplates/form
[11] http://www.puldb.ru/db/plates/index.php

Table 1
Photometry of GR 290 from Archival Plates

Plate no.	Date	JD	Emulsion	exp	rms	Slope	mag	Band	Remarks
				(1)	(2)	(3)			(4)
Hamburg									
S00332	1914 Sep 21	2420397	Hauff-Ultra	30	0.08	1.03	18.4	*B*	poor
S02358	1920 Oct 18	2422616	unknown	94	0.07	0.99	18.2	*B*	good
S02396	1920 Nov 12	2422641	Agfa-Isorapid	40	0.12	0.95	18.4	*B*	poor
S02436	1921 Feb 09	2422730	Agfa-Isorapid	40	0.18	1.03	17.9	*B*	poor
S02587	1921 Sep 09	2422942	Hauff-Ultra	114	0.13	1.11	18.5	*B*	fair
S02676	1921 Nov 24	2423018	Agfa-Isorapid	60	0.12	0.92	18.5	*B*	fair
S02982	1922 Nov 18	2423377	Agfa-Isorapid	30	0.12	1.02	18.4	*B*	fair
S04042	1928 Nov 09	2425560	Agfa-Astro-Inhalo	60	0.10	1.13	18.4	*B*	good
S04295	1930 Aug 24	2425483	Agfa-Astro-Inhalo	47	0.08	1.09	18.4	*B*	good
Pulkovo									
K235	1935 Nov 16	2428123	unknown	60	0.05	0.78	>16.5	*B*	not visible
K397	1937 Sep 30	2428807	unknown	100	0.28	1.20	18.67	*B*	faint
K412	1937 Oct 07	2428814	unknown	90	0.20	1.02	18.45	*B*	faint
K413	1937 Oct 07	2428814	unknown	105	0.08	0.84	17.95	*B*	faint
K508	1938 Nov 27	2429230	unknown	66	0.12	0.84	17.93::	*B*	very faint
K510	1938 Dec 17	2429250	unknown	80	0.08	1.09	18.54	*B*	very faint
Heidelberg									
D0154	1907 Aug 08	2417795	unknown	35	0.10	1.31	18.19	*B*	faint
D0169	1908 Aug 12	2417799	unknown	124	0.10	1.31	>17.5	*B*	not visible
D0359	1908 Jul 25	2418165	unknown	40	0.10	1.98	18.85	*B*	faint
D1615	1917 Dec 10	2421572	unknown	40	0.15	1.00	17.79	*B*	faint
D1616	1917 Dec 17	2421579	unknown	40	0.21	1.04	17.97	*B*	faint
D1617	1917 Dec 17	2421579	unknown	40	0.11	1.04	>17.5	*B*	not visible
D1631	1918 Jan 30	2421623	unknown	40	0.13	1.35	>17.5	*B*	not visible
D1632	1918 Jan 30	2421623	unknown	40	0.20	1.54	>17.5	*B*	not visible
D2118	1920 Aug 15	2422551	unknown	60	0.19	1.46	>17.5	*B*	not visible
D2119	1920 Aug 15	2422551	unknown	70	0.20	1.42	>17.5	*B*	not visible
D2485	1922 Oct 14	2423341	unknown	90	0.12	1.02	17.90	*B*	visible
D2498	1922 Oct 25	2423352	unknown	64	0.20	1.48	18.40	*B*	faint
Yerkes									
Ry-8:	1901 Aug 15	2415613	unknown	210	0.14	⋯	18.33	*B*	⋯
scanMP	1902 Sep 04	2415999	unknown	240	0.10	⋯	18.50	*B*	⋯
G107a	1910 Aug 06	2418890	unknown	510	0.10	⋯	18.26	*B*	60” Mt Wilson
R-3481:	1916 Sep 19	2421127	unknown	50	⋯	⋯	>17.95	*B*	not visible
R-3518:	1916 Dec 09	2421208	unknown +W12	240	⋯	⋯	>14.81	*V* ?	very dark plate
R-5478	1936 Nov 10	2428484	I-O	30	0.5	⋯	17.75	*B*	poor
R-5523:	1937 Jan 10	2428545	I-C+ red	60	⋯	⋯	>16.95	*V–R*	poor
R-5531:	1937 Jan 15	2428550	I-O	37	⋯	⋯	>17.95	*B*	not visible
R-5614:	1938 Oct 24	2429197	Agfa pan+yellow	60	⋯	⋯	>14.95	*V*	not visible
R-5616:	1938 Oct 24	2429197	Agfa pan+yellow	60	⋯	⋯	>14.95	*V*	not visible
R-5618:	1938 Oct 27	2429200	E-40	5	⋯	⋯	>15.43	*B*	not visible
R-5621:	1938 Oct 27	2429200	unknown	5	⋯	⋯	>15.45	*B*	not visible
R-5625:	1938 Nov 29	2429233	Agfa SPP+#28	40	⋯	⋯	>14.59	*R*	not visible
cl 204	1947 Sep 13	2432442	unknown	402	⋯	⋯	>17.95	*B*	not visible
vB9404	1952 Oct 12	2434299	⋯	⋯	0.06	⋯	18.40	*B*	
Palomar									
POSS-IE	1949 Dec 21	2433272	103aE+plexi	45	0.15	2.11	18.68	*R*	⋯
Quick-V	1982 Oct 18	2445261	IIaD+W12	20	0.06	1.86	17.81	*V*	⋯
POSS-IIB	1991 Sep 30	2448530	IIIaJ+GG395	60	0.05	2.58	16.54	*B*	⋯
POSS-IIR	1991 Oct 05	2448535	IIIaF+RG610	75	0.06	2.66	16.04	*R*	⋯
Asiago									
5624	1972 Sep 16	2441577	103aO+GG13	30	0.18	1.72	17.25	*B*	good
5831	1972 Nov 07	2441629	103aD+GG14	20	0.08	⋯	17.43	*V*	good
6804	1973 Oct 27	2441983	103aO+GG13	20	0.21	1.93	17.15	*B*	good
6940	1973 Dec 15	2442032	103aD+GG14	30	0.13	⋯	17.83	*V*	good
11699	1982 Oct 14	2445257	103aO clear	30	0.19	1.78	16.70	*B*	high background
12338	1983 Nov 28	2445667	103aD+GG14	30	0.12	⋯	>17.60	*B*	not visible

temperatures of the star, is all the time dominated by electron scattering. In fact, in agreement with the observed and theoretical continuum energy distribution of WN stars (Morris et al. 1993), we also expect the slope of the blue-visual continuum of GR 290 to be nearly independent of T_{eff} during its recent WN phase. Through the end of 2015, we measured

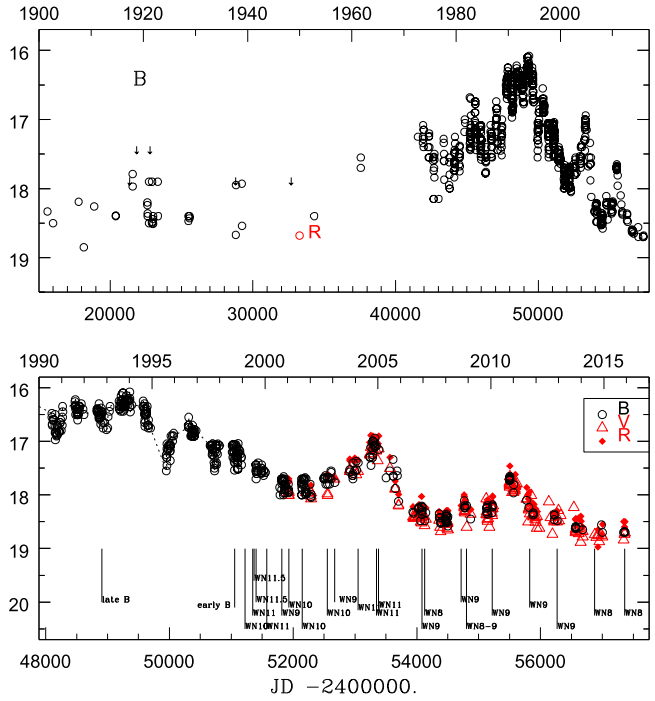

Figure 1. Upper panel: the historical light curve of GR 290 in the *B*-filter from 1901 to 2015. Some upper limits and the *R* magnitude from the 1949 POSS plate are also reported. Lower panel: a close up of the light curve since the 1990 brightest phase obtained from the *B*, *V*, *R* observations given in Table 3. The spectral types derived from the spectroscopic observations are marked.

two additional *U*-band magnitudes: $U = 17.98 \pm 0.08$ (November 14) and 17.78 ± 0.1 (December 11). The corresponding $(U - B)$ color index is the same within the errors as that we obtained in 2004 December (Viotti et al. 2006) when we derived $U = 16.22$ and $B = 17.09$. The fact that in spite of the large luminosity difference between the two epochs, the blue-ultraviolet color index did not significantly change further supports to the above conclusion.

3. THE SPECTRUM OF GR 290

The first recorded spectrum of GR 290 was taken by Thomas Szeifert at Calar Alto on 1992 October 15, when the star was near its absolute luminosity maximum with $B = 16.5$. According to the analysis of Szeifert (1996), this early spectrum is most likely to be of late-B spectral type. However, the next spectrum (1994), obtained in the 5500–7600 Å range at the SAO Russian 6 m telescope, when the star was still in its photometric maximum, led Sholukhova et al. (1997) to suggest that Romano's star could have been a WN because of the very broad He I 6678 A line. After the 1992–1994 maximum, GR 290 started to become fainter and hotter. In 1998 September, when the magnitude had already faded to about $B = 17.5$, the spectrum of GR 290 displayed weak [N II] emissions and strong He I lines with P Cygni profiles consistent with a WN10-WN11 spectral type (Fabrika et al. 2005).

The following spectral evolution until 2010 was described in detail by Viotti et al. (2007), Maryeva & Abolmasov (2010), Polcaro et al. (2011), Sholukhova et al. (2011), and Humphreys et al. (2014). As illustrated in the lower panel of Figure 1, the spectrum of GR 290 was WN9h–WN10h during the 2000–2003 minimum, then became WN11h at the following 2004 maximum. A new hot (WN8h–WN9h) phase was recorded at the 2007 minimum. The subsequent apparent luminosity increase in 2010 was marked only by a slightly cooler spectrum (WN9h–WN10h), while a new hot (WN8h–WN9h) phase took place during the last minimum phase that is still ongoing.

New observations were obtained since 2010 with the BFOSC camera mounted on the 1.52 m Loiano telescope and with the SCORPIO camera available with the SAO Russian 6 m telescope.[12]

In Figure 3, we present a selection of the spectra acquired since 2010 in the range of 4500–4800 Å, which contains the most diagnostic lines for spectral typing. In Table 3, we report the spectral types together with the corresponding *V* magnitudes and the equivalent widths of some H and He lines.

The spectral evolution of the star during recent years is mainly described by the changes in the equivalent width of helium lines and of the broad blend of emission lines around 4650 Å (the so-called f-feature). Neutral and ionized helium lines have opposite behavior. The hydrogen Balmer lines, Hα and Hβ are irregularly variable, but their variations do not seem to follow the light curve, except for a probable gradual weakening in recent years. In particular, during the 2003–2014 period, the Hα/Hβ equivalent width ratio did not significantly vary around a mean value of 4.2. Figure 4 illustrates the time evolution of the hydrogen emission lines (top panel) and the ratio Hα/Hβ (lower panel) during the 2002–2015 period. The lower panel also shows the equivalent width ratio (He II 4686)/(He I 5876), which is smaller when the stellar apparent luminosity is higher. Furthermore, the apparently dumped EW oscillation of both the He II 4686 Å line and the 4686/5876 ratio might suggest a trend of increasing temperature.

The He II 4686 Å and He I 5876 Å lines have been used by Crowther & Smith (1997) to distinguish stars with different spectral types. Polcaro et al. (2011) used the equivalent widths diagrams EW(5876) versus EW(4686) to mark the path of GR 290 through the WN sub-classes during its recent luminosity variations. Since 2010 January, the star has moved in the Crowther and Smith diagram toward the WN8 locus and, from 2013 December to 2015 December, its representative point is well inside the WN8 locus, as it was at the beginning of 2008 during the previous minimum (see Figure 5).

The growing excitation temperature of WR stars from late to earlier subtypes is best described by the intensity of the emission lines between 4600 and 4700 Å. The blend forming the f-feature as well as the He II 4686 Å emission becomes prominent when the star is fainter, as was ascertained by Polcaro et al. (2011) and shown in Figure 3. In order to quantitatively study this behavior, we have measured the equivalent width of the emission in the 4600–4700 Å range, avoiding the lower excitation He I 4713 Å line, which is too strong in the later WN spectral types. In Figure 6, we plot the EW (in logarithm) of both the He II 4686 Å line and the 4600–4700 Å blend as a function of the *V* magnitude. The 4600–4700 Å blend presents a marked linear correlation with the *V* magnitude in an ample luminosity range with a mean slope of 0.544 ± 0.027. We remark that this correlation does not vary, within the errors, during three different optical variability cycles. For the He II line, the linearity fails when the

[12] We used both public data from the SAO RAS archive (http://www.sao.ru/oasis/cgi-bin/fetch) and the data acquired by O. Maryeva during dedicated observations.

Table 2
New Photometric Observations of GR 290

Date	*B*	*V*	*R*	*I*	Obs[a]
2010 Dec 10	⋯	17.95 .10	⋯	⋯	Greve
2010 Dec 28	⋯	17.88 .07	⋯	⋯	ARA
2011 Jan 03	17.96 .05	17.95 .05	17.73 .04	⋯	Loiano
2011 Jan 05	17.81 .05	⋯	⋯	⋯	SSON
2011 Jan 08	⋯	17.92 .05	⋯	⋯	ARA
2011 Jan 23	⋯	17.92 .07	⋯	⋯	Greve
2011 Feb 05	⋯	17.80 .10	⋯	⋯	Greve
2011 Feb 05	⋯	17.82 .06	⋯	⋯	ARA
2011 Feb 26	⋯	17.79 .10	⋯	⋯	ARA
2011 Jul 30	⋯	18.08 .10	⋯	⋯	ARA
2011 Aug 02	18.10 .07	18.07 .06	17.86 .04	⋯	Loiano
2011 Aug 28	⋯	18.50 .09	⋯	⋯	ARA low quality
2011 Sep 07	18.23 .09	18.26 .06	18.07 .03	⋯	Loiano
2011 Sep 21	⋯	18.35 .09	17.94 .12	⋯	ARA
2011 Oct 02	⋯	18.22 .08	⋯	⋯	ARA
2011 Oct 05	⋯	18.17 .10	⋯	⋯	ARA
2011 Oct 29	⋯	18.22 .07	⋯	⋯	ARA
2011 Nov 15	⋯	18.36 .05	18.39 .04	18.17 .02	Loiano
2011 Nov 26	⋯	18.33 .08	18.18 .06	⋯	ARA
2011 Dec 17	⋯	18.45 .09	⋯	⋯	ARA
2011 Dec 23	⋯	18.51 .09	⋯	⋯	ARA
2011 Dec 23	⋯	18.44 .06	⋯	⋯	ARA
2011 Dec 26	⋯	18.42 .08	18.26 .08	⋯	ARA
2012 Jan 21	⋯	18.31 .09	⋯	⋯	ARA
2012 Feb 25	⋯	18.62 .12	⋯	⋯	ARA
2012 Jul 28	⋯	18.19 .09	⋯	⋯	ARA
2012 Aug 24	⋯	18.42 .09	⋯	⋯	ARA
2012 Oct 21	18.39 .05	18.49 .04	18.37 .05	18.46 .08	IAC80
2012 Dec 12	18.47 .06	18.52 .06	18.30 .04	⋯	Loiano
2012 Dec 30	⋯	18.29 .08	⋯	⋯	ARA
2013 Jan 07	⋯	18.48 .08	⋯	⋯	ARA
2013 Feb 04	⋯	18.38 .07	⋯	⋯	ARA
2013 Sep 04	⋯	18.23 .10	⋯	⋯	ARA
2013 Oct 01	⋯	18.68 .10	⋯	⋯	IAC80
2013 Oct 02	18.62 .02	18.66 .03	18.46 .03	18.81 .18	IAC80
2013 Oct 04	18.62 .03	18.70 .03	18.46 .03	18.71 .07	IAC80
2013 Oct 05	18.60 .02	18.67 .02	18.45 .03	18.69 .07	IAC80
2013 Nov 26	18.60 .05	18.72 .06	18.43 .05	⋯	Loiano
2013 Dec 23	⋯	18.88 .14	18.40 .12	⋯	ARA
2013 Dec 23	⋯	⋯	18.40 .12	⋯	ARA
2013 Dec 30	⋯	18.68 .13	⋯	⋯	SSON
2014 Jan 01	⋯	⋯	18.49 .04	⋯	Loiano
2014 Jan 25	18.65 .07	18.68 .04	18.60 .04	⋯	Loiano
2014 Aug 08	⋯	⋯ 18.74 .10	⋯	⋯	ARA
2014 Aug 31	⋯	⋯ 18.79 .10	⋯	⋯	ARA
2014 Sep 27	⋯	⋯	18.97 .13	⋯	ARA
2014 Oct 04	⋯	18.76 .05	18.65 .03	⋯	Loiano
2014 Oct 20	⋯	18.87 .12	⋯	⋯	ARA
2014 Nov 21	⋯	18.75 .12	⋯	⋯	ARA
2014 Dec 11	18.67 .07	18.78 .07	18.55 .05	⋯	Loiano
2015 Aug 21	⋯	18.77 .08	⋯	⋯	ARA
2015 Nov 06	⋯	18.78 .08	⋯	⋯	ARA
2015 Nov 18	18.70 0.03	18.84 .04	18.50 0.04	⋯	Loiano[b]
2015 Dec 02	18.64 0.05	18.73 .05	18.60 0.06	18.74 0.07	Loiano
2015 Dec 10	18.70 0.04	18.71 .04	18.50 0.04	⋯	Loiano[b]

Notes.
[a] Observatories: Greve: 30 cm telescope at Greve in Chianti (Firenze). ARA: 37 cm telescope of the Associazione Romana Astrofili at Frasso Sabino (Rieti). Loiano: 1.52 m telescope at the Loiano station of the Bologna Astronomical Observatory-INAF. SSON: the Sierra Stars Observatory Network in Mount Lemmon (Arizona). IAC80: 80 cm Tenerife telescope of the Astrofisico de Canarias.
[b] On 2015 November 14, $U = 17.98 \pm 0.08$, on 2015 December 10, $U = 17.70 \pm 0.1$.

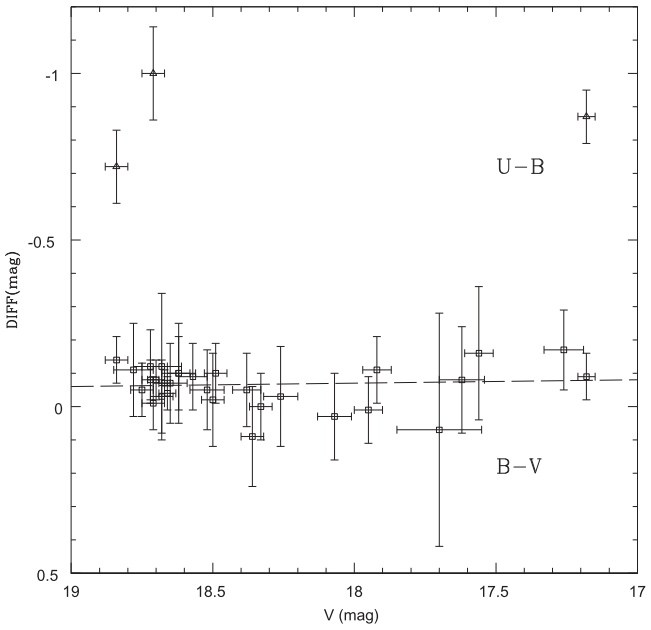

Figure 2. $(B - V)$ and $(U - B)$ color indices vs. the V magnitude during 2003 February–2015 December. The mean $(B - V)$ color index is indicated by the dotted line.

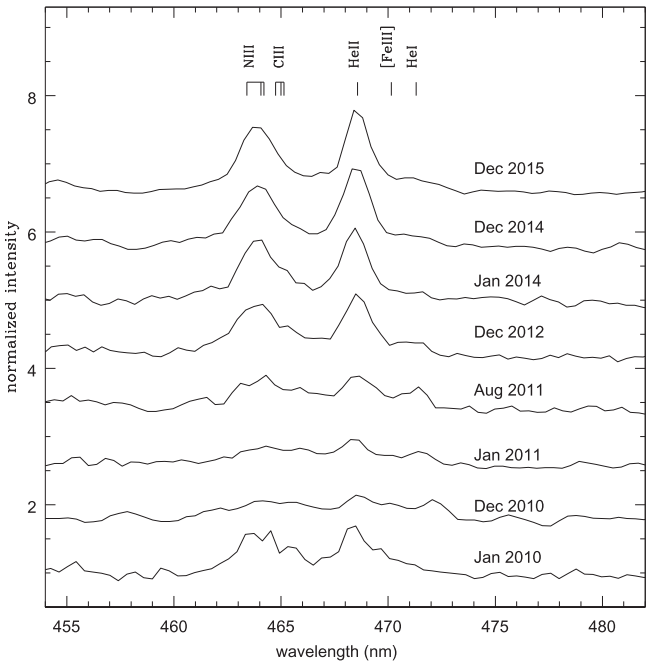

Figure 3. Time evolution of the spectrum of GR 290 near the *f*-band between 2010 January and 2015 December. The successive spectra are vertically shifted.

star is bright, possibly because of the large uncertainty on the lowest equivalent widths.

4. PHYSICAL PARAMETERS OF GR 290

Maryeva & Abolmasov (2012a) and Clark et al. (2012), using the CMFGEN atmospheric modeling code (Hillier & Miller 1998), have derived the physical parameters of GR 290 using spectra taken in 2005 February ($V = 17.2$) and 2007 October–2008 January ($V = 18.6$), and in 2010 September ($V = 17.9$). Presently, we have at our disposal many spectra of the star collected mainly at the Loiano Observatory and at the SAO, covering the period of 2002 October–2014 December when the star displayed an ample range of variation in visual luminosity. This time interval covers two light maxima and three minima. In order to see how the parameters of GR 290 changed with time, we have modeled the most representative spectra with the best quality obtained during this period.

We have applied the same procedure as Maryeva & Abolmasov (2012a) and have constructed nine models. Details on the procedure may be found in Maryeva & Abolmasov (2012a) and are not repeated here except where necessary.

Every model is defined by a hydrostatic stellar radius R_*, luminosity L_*, mass-loss rate $\dot{M}$, filling factor f, wind terminal velocity v_∞, stellar mass M_*, and by the abundances Z_i of the element species.

We started modeling by fitting the spectra obtained in 2005 January during a phase of maximum brightness and in 2008 December. These spectra are most suitable as having the widest spectral range and the best resolution among our spectra. Then, for every spectrum, we have calculated a few models giving similar fits with slightly different mass-loss rates, velocities, temperatures, radii, and filling factors. The uncertainties reported below include the range of parameters of the models. We assumed that element abundances do not change with changing phases. Thus we used the abundances derived for the 2008 December spectrum to fit all of the remaining data.

Various attempts to derive the H/He abundance ratio gave a large range of possible values from 1.5 to 1.9; differences between the models are not evident unless all the others parameters are fixed. Ultimately, we decided to assign a value of 1.7 to the H/He ratio. We estimated the abundances of carbon $(\mathrm{N(C)/N(He)} = 1^{+0.4}_{-0.3} \times 10^{-4})$ and nitrogen $(\mathrm{N(N)/N(He)} = 3^{+1.5}_{-1} \times 10^{-3})$ by fitting the WR blue bump of the blend at 4630–4713 Å. The determination of the oxygen fraction is a more difficult task since there are no oxygen emission lines in the spectrum of GR 290. However, we noticed that the intensity of the He II lines decreases when we include oxygen in our model. Thus we estimated the oxygen abundance indirectly by fitting the He II lines and obtained $\mathrm{N(O)/N(He)} = 2^{+2}_{-1} \times 10^{-4}$. For the abundances of Ar, S, and Ne, we used those of M33 from Magrini et al. (2010). For the abundances of other elements (Mg, Al, Si, Ca, and Fe), we assumed a value of half solar as the metallicity of M33 is low. We compared several models and concluded that the abundances of these elements do not affect model spectra significantly.

CMFGEN allows us to build the models with different velocity laws describing the radial dependence of the wind velocity. Often the same spectrum may be equally well described by either a simple β law or a more complex double-β profile, yielding different values of luminosity and temperature. In this work, our main task is to track the changes of stellar parameters over time. Due to the lack of theoretical works on this topic, it is difficult to say now which velocity profile is more physically justified; this is a question we leave for a separate publication. Here we found it sufficient to use the same simple wind velocity law with $\beta = 1$ for all models. Due to the fact that the profiles of spectral lines are very sensitive to the value of the terminal velocity, we can estimate v_∞ using even low-resolution spectra. At minimum brightness, we used the P Cyg profiles of the He I triplet lines (such as $\lambda\lambda$3889 Å, 4025 Å, 4471 Å, and 6678 Å) and derived $V_\infty = 400\ \mathrm{km\ s^{-1}}$. At

Table 3
Emission Line Measurements in the Spectrum of GR 290

Date	V	$H\alpha$	$H\beta$	Band	468.6	587.6	sp.typ.	Obs	Remarks
(1)	(2)	(3)	(4)	(5)	(6)	(7)	(8)	(9)	(10)
1992 Oct 06	16.4*	47.7 1.0	10.0 1.0	⋯	⋯	1.25 0.1	late-B	CalarA	468 np
2002 Oct 04	17.98	113.0 3.0	23.0 0.4	30.0 3.0	12.0 3.0	18.0 2.0	WN10h	SAO-M	⋯
2003 Feb 02	17.70	97.6 3.0	27.3 0.5	15.5 1.0	6.6 1.0	22.3 1.0	WN10.5h	Loiano	⋯
2004 Feb 14	17.56	100. 2.0	26.4 1.0	11. 1.0	1.3 0.5	22.2 2.0	WN11h	Ekar	468 v.un.
2004 Nov 12	17.18	97.3 2.0	24.0 1.0	7.0 2.0	⋯	21.0 1.0	WN11h	SAO-M	468 n.m.
2004 Dec 07	17.18	113. 2.0	27.0 0.5	6.5 0.7	1.4 0.3	23.7 0.5	WN11h	Ekar	468 uncer.
2005 Jan 13	17.26	111. 3.0	27.5 1.0	6.4 1.5	1.1 0.5	21.5 0.5	WN11h	Loiano	468 v.un..
2005 Feb 06	17.24	112.5 0.5	26.0 0.3	7.6 1.0	1.4 0.3	25.5 0.7	WN11h	SAO-S	⋯
2005 Aug 31	17.5	120.0 5.0	26.7 0.5	18.5 1.5	7.0 0.8	26.0 1.5	WN10h	SAO-S	⋯
2005 Nov 08	17.6	150.0 7.0	36.7 1.0	30.3 0.5	11.0 0.7	34.5 0.8	WN9h	SAO-S	⋯
2006 Aug 03	18.43	⋯	25.1 0.7	37.5 1.0	11.2 0.5	⋯	WN8h	SAO-S	⋯
2006 Sep 29	18.4	⋯	22.1 0.5	31.1 0.5	9.0 0.3	⋯	WN8h	WIYN	⋯
2006 Nov 21	18.50	144. 7.0	32. 2.0	47. 5.	19. 3.0	33. 3.0	WN8h	Loiano	low
2006 Dec 14	18.55	129. 7.0	27.2 1.0	39.9 0.5	17.5 0.3	36.1 1.5	WN9h	Loiano	⋯
2007 Jan 29	18.57	119. 4.0	27.3 1.0	36.5 3.0	13.1 2.0	26.9 0.5	WN8h	Loiano	⋯
2007 Aug 10	18.5	⋯	24.7 0.5	44.6 0.5	16.8 1.0	⋯	WN8h	SAO-S	⋯
2007 Oct 06	18.6	⋯	24.3 0.3	46.0 1.0	16.6 0.5	⋯	WN8h	SAO-S	⋯
2008 Jan 08	18.62	⋯	23.7 0.3	43.0 2.0	14.4 1.0	⋯	WN8h	SAO-S	⋯
2008 Jan 10	18.62	109.6 1.0	⋯	⋯	⋯	26.3 0.3	WN8h	SAO-S	⋯
2008 Jan 23	18.65	128. 5.0	29.0 3.0	55.8 5.0	27.2 3.0	30.0 2.0	WN8h	Loiano	465 uncer.
2008 Feb 07	18.65	132. 4. 0	30.6 1.0	44.0 3.0	21.3 1.0	27.5 1.0	WN8h	Loiano	⋯
2008 Sep 08	18.44	115. 4. 0	28.1 0.5	33.4 1.5	12.8 0.3	30.1 1.0	WN9h	Loiano	⋯
2008 Dec 04	18.31	126. 2. 0	25.0 0.5	36.6 0.5	13.1 0.3	28.8 0.5	WN9h	WHT	⋯
2009 Feb 15	18.36	117. 3. 0	27.9 0.3	38.5 2.0	12.8 0.5	31. 2.	WN9h	Loiano	low q
2009 Oct 09	18.36	115.2 1. 5	26.0 0.5	38.8 1.0	18.4 1.5	27.8 0.5	WN9h	SAO-S	⋯
2010 Jan 21	18.38	114. 2. 0	27.7 0.4	32.5 1.5	13.8 0.7	26.2 0.4	WN9h	Loiano	low q.
2010 Dec 06	17.66	⋯	26.2 0.3	20.1 0.5	7.6 0.5	⋯	WN10h	SAO-S	⋯
2010 Dec 18	17.93	106. 2. 0	28.2 0.5	21.2 2.5	8. 2.	32.5 2.0	WN10h	Loiano	468 uncer.
2011 Jan 03	17.95	114. 2. 5	29.0 0.5	16.6 1.5	6.9 0.5	25.6 0.3	WN10h	Loiano	⋯
2011 Aug 03	18.07	114.5 1. 0	29.2 0.5	23.4 1.5	8.0 0.7	30.5 0.5	WN10h	Loiano	⋯
2011 Sep 20	18.26	122. 5. 0	30.8 0.3	31.7 1.0	13.0 0.5	34.6 0.5	WN9h	Loiano	⋯
2012 Dec 09	18.50	111. 2. 0	23.5 0.3	39.0 2.0	16.3 0.5	30.0 1.0	WN8h	Loiano	⋯
2013 Nov 27	18.72	98.5 1. 0	23.1 0.3	44.7 0.5	21.4 0.5	23.2 0.5	WN8h	Loiano	⋯
2014 Jan 01	18.68	94.2 2. 0	22.4 0.2	38.7 2.0	17.6 0.5	20.3 1.0	WN8h	Loiano	⋯
2014 Aug 03	18.74	⋯	20.0 0.3	45.3 1.0	14.4 0.1	⋯	WN8h	SAO-S	⋯
2014 Dec 11	18.78	92.9 0. 7	21.1 1.0	44.5 0.5	20.2 0.5	18.7 0.3	WN8h	Loiano	⋯
2014 Dec 30	18.74	94.0 2. 0	21.9 0.5	43.9 1.5	20.0 0.5	20.8 1.0	WN8h	Loiano	⋯
2015 Jan 26	18.7	83. 2.	23.5 1.5	50. 5.	24.1 1.5	18.4 1.0	WN8h	Loiano	low q.
2015 Feb 19	18.61	⋯	19.6 1.0	42.1 5.0	16.3 1.0	⋯	WN8h	SAO-S	low q.
2015 Dec 02	18.64	88.3 0.8.	20.5 1.3	47.0 3.	21.7 1.1	22.4 0.7	WN8h	Loiano	⋯
2015 Dec 10	18.70	89.5 1.0	20.5 0.5	35.0 0.7	20.0 0.7	19.5 0.8	WN8h	Loiano	⋯

Note. (1) year, month, day. (2) V magnitude (B for the 1992 spectrum). (3) EW and error of Hα excluding the nearby [N II] doublet. (4) EW and error for Hβ. (5) EW of the 4600–4700 Å, emission blend excluding He I 4713 Å. (6) EW of the He II 4686 line. (7) EW of He I 5876. (8) spectral type. (9) Observatory: CalarA.: Calar Alto Obs. Ekar: Cima Ekar (Padova Observatory). Loiano: Loiano Station (Bologna Observatory). SAO-M/-S: 6 m Special Astronomical Observatory equipped with MPFS (M) or SCORPIO (S) cameras. WHT: 4 m William Hershel Observatory. WIYN 3.5 m Observatory (Kitt Peak). (10) remarks: 486: He II 4686 Å line; 465: the 4600–4700 Å emission blend; np: not present; n.m.: not measurable; (v.) uncer: (very) uncertain; low q.: low quality spectrum (noisy, bad skv).

maximum brightness, we used the emission line fits and found $V_\infty = 200$–$250\,\mathrm{km\,s^{-1}}$. Thus V_∞ changes from the hot phase to the cool phase, and this changing is real. Indeed, if at maximum brightness the velocities were equal to $400\,\mathrm{km\,s^{-1}}$, then we would have detected P Cyg profiles even in our low-resolution spectra. However, P Cyg profiles are not observed at maximum brightness in the spectrum obtained in 2005 January with spectral resolution $\Delta\lambda = 3.5$ Å.

For measuring $T_{\rm eff}$ with CMFGEN, we compared the intensities of different ion lines (He I, II; C III, IV; N II, III; Si III, IV), i.e., we used the traditional ionization-balance method. For the C ionization structure, we used the C III $\lambda\lambda$4647-50 Å diagnostic lines. For the N: N II 4601-07-30-43 Å, N III 4510-15-18-24-31-35-47 Å, N III 4634-40 Å. The Si ionization structure was constrained through the relative strength of Si III and Si IV lines, using lines of Si III 4553-4568-4575 Å and Si IV 4088-4116 Å. By cross-checking all these indicators, we estimated an uncertainty of ± 1.000 K.

To estimate the luminosity of the object, hence the stellar radius, the magnitudes of the star were calculated in the B and V filters from the model spectra and compared with observations. The model $(B-V)_0$ is determined by the temperature, which was estimated as described above; this model color is then compared with the observed $B-V$ from which the comparison of the reddening is determined.

The result is that the model $(B-V)_0$ is consistent with observed $B-V$ only if $E(B-V) < 0.08$, assuming for M33 a distance of $D = 847 \pm 60$ kpc (Galleti et al. 2004).

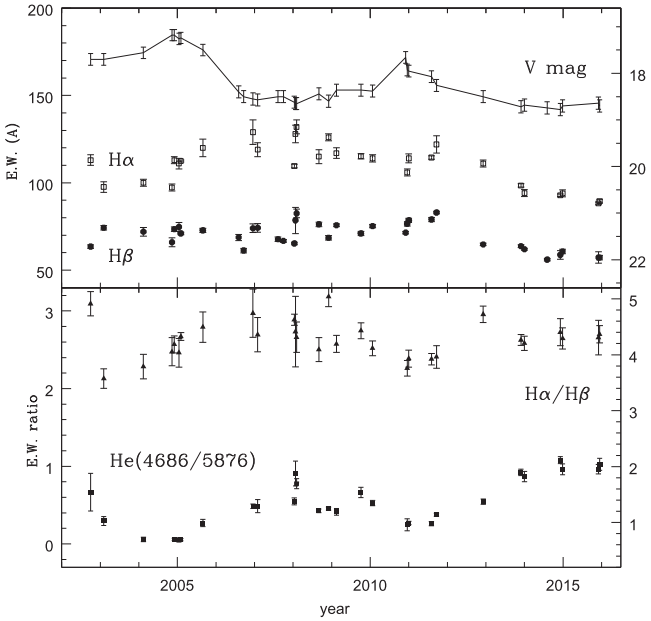

Figure 4. Equivalent width (in Å) and ratios of the main emission lines in the spectrum of GR 290 during 2002–2015. Top panel: e.w of Hα (open squares) and of Hβ (filled circles, multiplied by 2.5). The corresponding V magnitude is shown for comparison (connected points, left scale). In this and in the following plots, only the EW derived from the Loiano and Cima Ekar Observatories have been plotted for homogeneity. Lower panel: ratio of the equivalent width of He II 4686 Å/He I 5876 Å (filled squares, left scale) and Hα/Hβ (filled triangles, right scale).

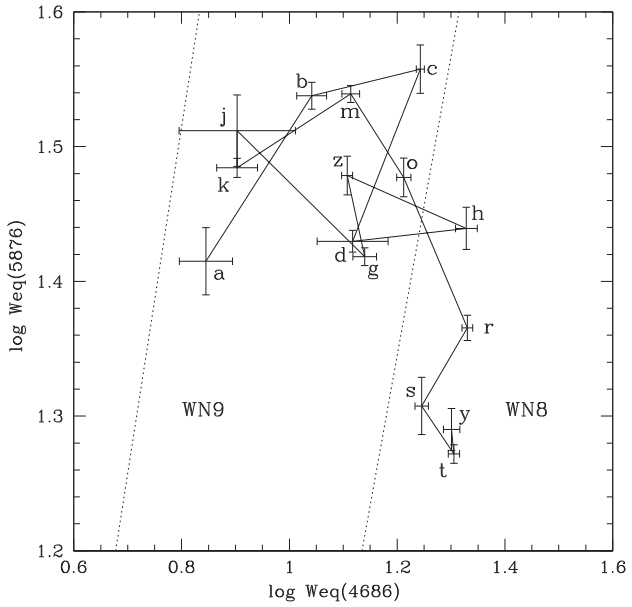

Figure 5. Time evolution of the equivalent width of He II 4686 Å and He I 5876 Å to mark the path of GR 290 through the WN sub-classes during its luminosity variations from 2005 August to 2015 December. The letters correspond to the following dates: a = 2005 August 31; b = 2005 November 08; c = 2006 December 14; d = 2007 January 29; h = 2008 February 07; z = 2008 September 08; g = 2010 January 21; j = 1010 December 18; k = 2011 August 03; m = 2011 September 20; o = 2012 December 09; r = 2013 November 27; s = 2014 January 01; t = 2014 December 11; y = 2015 December 11.

Actually, the Galaxy foreground extinction is $E(B-V) = 0.052$ (according to the NED extinction calculator, Schlegel et al. 1998) and the intrinsic extinction in M33 is

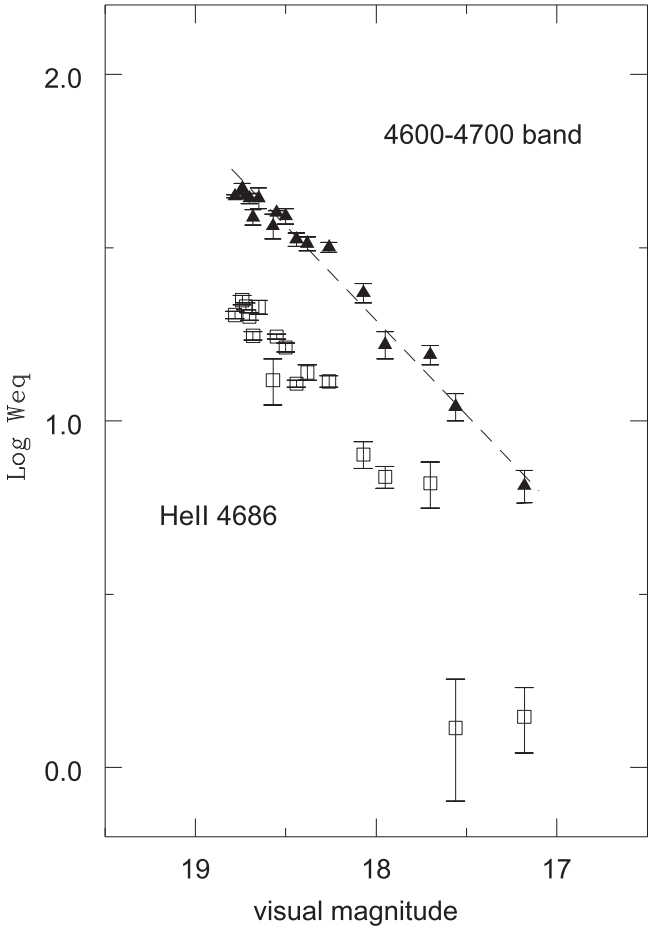

Figure 6. Logarithm of the equivalent width of the He II 4686 Å line (open squares) and the 4600–4700 Å emission feature (triangles) vs. visual luminosity during 2003 January–2015 December. The fit of the data points described in the text is shown.

negligible according to the detailed dust maps by Hippelein et al. (2003).

Furthermore, $E(B-V)$ have also been computed for four close stars whose magnitudes and spectral types are given in Massey et al. (2006). The closest star, a B0.5Ib, has $E(B-V) = 0.06$, nearly the same as found for GR 290.

Finally, we have computed models with extinction up to $E(B-V) = 0.15$, as assumed by Humphreys et al. (2014). Of course, higher extinction would imply a significant increase of the luminosity. However, in all the minimum phases, GR 290 would lie still outside the instability strip of LBV stars.

The mass-loss rate was obtained by reproducing the intensities of the strongest lines—namely, those of hydrogen, helium, and nitrogen.

The parameters of GR 290 were also obtained by Maryeva & Abolmasov (2012a) during the maximum brightness in 2004–2005. For this goal, these authors used a spectrum obtained in 2005 February at the Russian 6 m telescope with spectrograph SCORPIO with spectral resolution $\Delta\lambda = 10$ Å. To reproduce that spectrum a volume-filling factor $f = 0.5$ was necessary. Clark et al. (2012) modeled the spectrum of Romano's star obtained in 2010 September when the V-band magnitude of the object was between 17.75 and 17.85. They also used the CMFGEN code; the best fit was obtained with $f = 0.25$. Since, in the current work, we used the spectrum

Table 4
Spectral Data of GR 290 Used to Construct the Models

Date	Obs.	Spectral Range	$\delta\lambda$ [Å]	S/N
2002 Oct	SAO-M	4250–6700	6	16
2003 Feb	Loiano	3650–8600	11	⋯
2005 Jan	Loiano	4150–6600	3.5	⋯
2006 Sep	WIYN[a]	4000–5100	⋯	⋯
2007 Oct	SAO-S	4000–5700; 5700–7500	5; 5	40; 20
2008 Dec	WHT	3000–10 000	0.8; 1.8	30; 20
2009 Oct	SAO-S	3700–7800	5	35
2010 Dec	SAO-S	4100–5800	5	60
2014 Aug	SAO-S	4000–5650	5	20

Note. $\Delta\lambda$ is spectral resolution. S/N is signal-to-noise ratio.
[a] Data taken from Clark et al. (2012).

obtained in 2005 January with better resolution ($\Delta\lambda = 3.5$ Å), we tried to fit the observed spectra with several values of the filling factor. We found that models with $f = 0.1$ well describe all spectra; $f = 0.2$ gives equally good results. The other parameters change very little with respect to the first case, the main difference, being in $T_{\rm eff}$, is always within the errors. Models with $f = 0.3$ give a worse fit for every other parameters. From the comparison of observed with model spectra, it is not clear which value of f is more correct. We assumed as final value $f = 0.15$.

Table 4 lists all spectroscopic observations of GR 290 used to construct the models. Details on the instrumental characteristics are described in Paper 1 and in Maryeva & Abolmasov (2012a). The observed spectra and the models themselves are shown in Figure 7. Table 5 lists the parameters of these models.

The accuracy of the derived estimates of luminosity and radius depends on several parameters, including the uncertainty of the distance and of the interstellar extinction. However, since the main scope of our work is to estimate the amplitude of the variation of the parameters and its accuracy, in Table 5, we only give the errors derived from the fitting procedure. It is worth noting that at maximum brightness He II and N III lines are absent (or very weak), thus our estimations give effective temperature in the range of 20–23 kK. This range of values of $T_{\rm eff}$ leads to a large scatter in the luminosities, which, at maximum brightness, results in the range $0.75–1 \cdot 10^6 L_{\odot}$.

We can see from Table 5 that the radius $R_{2/3}$, where the Rosseland optical depth is equal to 2/3 and is as low as 22–26 $R_{\odot}$ near the minima and increases up to 63 $R_{\odot}$ during the 2005 maximum. On the other hand, the temperature at $R_{2/3}$ decreases from 31 to 33 kK (with WN8-9h spectral type) to 25 kK (WN11h). The nature of the stellar wind significantly changes, being much denser and slower during the eruption in 2005. Figure 8 illustrates the structure of the wind-filled envelope of GR 290 during different luminosity phases. Note that the $R_{2/3}$ surface moves deeper in the wind during the minima. For comparison, Figure 8 shows the structure of the wind of two WN8h stars: FSZ35 (Maryeva & Abolmasov 2012b) and WR156 (Maryeva et al. 2013), belonging to M33 and our Galaxy, respectively. It is clear that the wind structure of GR 290 during the minimum of brightness is fairly similar to the one of typical WN8h (non-variable) stars.

Our estimates are consistent with those by Clark et al. (2012) within the errors, with the exception for the luminosity. It must be noted that Clark et al. (2012) assumed a distance to M33 of 964 kpc, while we adopted a distance of 847 kpc. Due to this difference in the assumed distances, we cannot directly compare the model luminosities, as the luminosity influences both the apparent magnitude of the star and the mass-loss rate, which is crucial for all other parameters.

The main result of this analysis is that the bolometric luminosity of GR 290 is variable, being higher during the phases of greater optical brightness. Previously, Polcaro et al. (2011) found a significant decrease in the bolometric luminosity between the 2005 maximum and the 2008 minimum. Later, Maryeva & Abolmasov (2012a) gave further proof that the bolometric luminosity of GR 290 has really decreased by about 40%. The present model fitting of a large sample of spectra obtained during two successive luminosity cycles definitely confirm their result and allows us to trace the recent path of the star in the Hertzsprung–Russell (H–R) diagram shown in Figure 9.

As a further check of the above result, we tried to construct models with constant bolometric luminosity, but the resulting model stellar magnitudes differ from the observed ones. For example, if we take $L_* = 6 \cdot 10^5 L\odot = \text{const}$ then the difference between the 2008 December model stellar magnitude and the observed one is about 0.2 mag. Such a difference might be due to photometric errors. However, for the 2005 February model such difference exceeds 0.7 mag, and this cannot be in any way attributed to photometric uncertainties. Therefore, we conclude that the bolometric luminosity variation is real.

5. THE EVOLUTIONARY STATE OF GR 290

5.1. GR 290 and the LBV Stars

As discussed in the previous sections, GR 290, from the observational point of view, shares some properties of the strongly active LBVs as classified by van Genderen (2001). However, GR 290 is different from all other known LBVs for being at any luminosity phase much hotter, since it presently exhibits a WN9-11h spectral type during brightness maxima and a WN8h spectral type at the minima. Also the spectral type shown by GR 290 during the 1992–94 absolute maximum (equivalent to B, probably late spectral type) is hotter than the ones of the majority of other LBVs, that usually have A phases. or even F spectral types during their maximum. Furthermore, if the present correlation between the visual magnitude and the spectral type had also been valid before 1960, GR 290 (its luminosity being weaker than $B = 17.5$ mag in all the recorded data) would have been much hotter than all the currently known dormant LBVs (all having an Ofpe—or WN 9-11—spectral type) also during its long lasting quasi-quiescent phase in the first half of the 20th Century.

Last, all the stars considered to be dormant LBVs thus far (but one: HDE326823, that was suggested to be in a post-LBV phase by Sterken et al. 1995) are placed near the lower boundary of the instability strip (Wolf 1989). On the contrary, the GR 290 representative point in the H–R diagram, as seen in Figure 9, is presently far from the instability strip.

We also stress that the spectral and luminosity variations of GR 290 in the last years occurred at a nearly constant $(B - V)$ color index, contrary to what is expected for an LBV.

It is thus unavoidable to conclude that presently there are no known LBV stars that can be directly compared with GR 290 in every aspect.

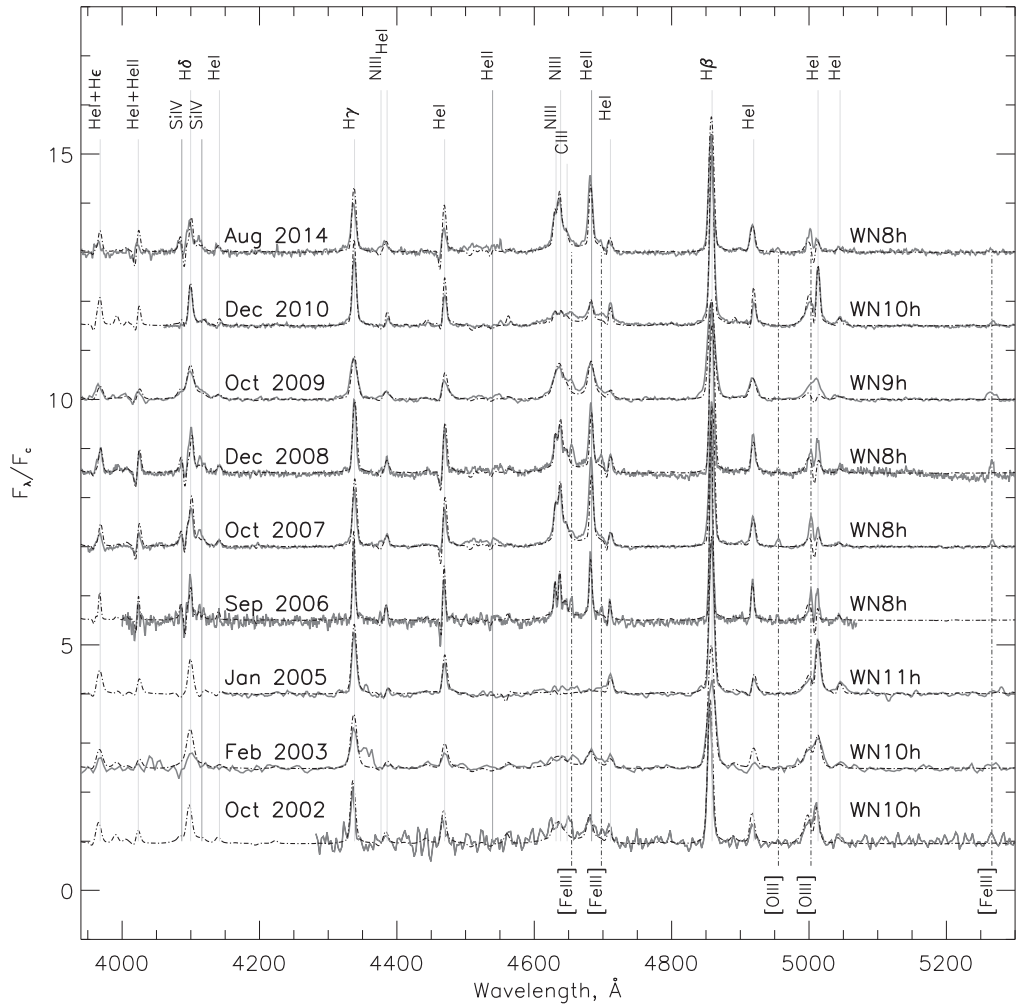

Figure 7. Normalized optical spectra of GR 290 compared with the best-fit CMFGEN models (dashed–dotted line). The model spectra are convolved with a Gaussian instrumental profile.

Table 5
Derived Properties of Romano's Star

Date	V (mag)	Sp. type	$T_{\rm eff}$ (kK)	$R_{2/3}$ ($R_\odot$)	L_*10^5 ($L_\odot$)	$\log L_*$ ($L_\odot$)	$\dot{M}_{cl}\,10^{-5}$ ($M_\odot$ yr^{-1})	f	v_∞ (km s^{-1})	H/He
2002 Oct	17.98	WN10h	28.0	39	8.0	5.90	2.4	0.15	250 ± 100	1.7
2003 Feb	17.70	WN10.5h	27.5	44	9.5	5.98	2.4	0.15	250 50	1.7
2005 Jan	17.24	WN11h	23.5[a]	61	10.05	6.02[a]	4.0	0.15	250 50	1.7
2006 Sep	18.4	WN8h	31.0	28	6.7	5.83	1.5	0.15	250 100	1.7
2007 Oct	18.6	WN8h	33.3	23.8	6.3	5.8	1.9	0.15	370 50	1.7
2008 Dec	18.31	WN8h	31.5	28.5	7.2	5.86	2.3	0.15	370 50	1.7
2009 Oct	18.36	WN9h	32.0	28.4	7.5	5.875	2.0	0.15	300 100	1.7
2010 Dec	17.95	WN10h	26.7	42	8.0	5.9	2.6	0.15	250 100	1.7
2014 Aug	18.74	WN8h	33.0	22.5	5.3	5.72	1.7	0.15	400 100	1.7
Errors			±1.0		±0.5		±0.3	±0.05		±0.2
2010 Sep[b]	17.8	WN10h	26	41.5		5.85	2.18	0.25	265	1.5

Notes. H/He indicates the hydrogen number fraction relative to helium, f is the filling factor.
[a] Errors for these values are given in the text.
[b] Data taken from Clark et al. (2012).

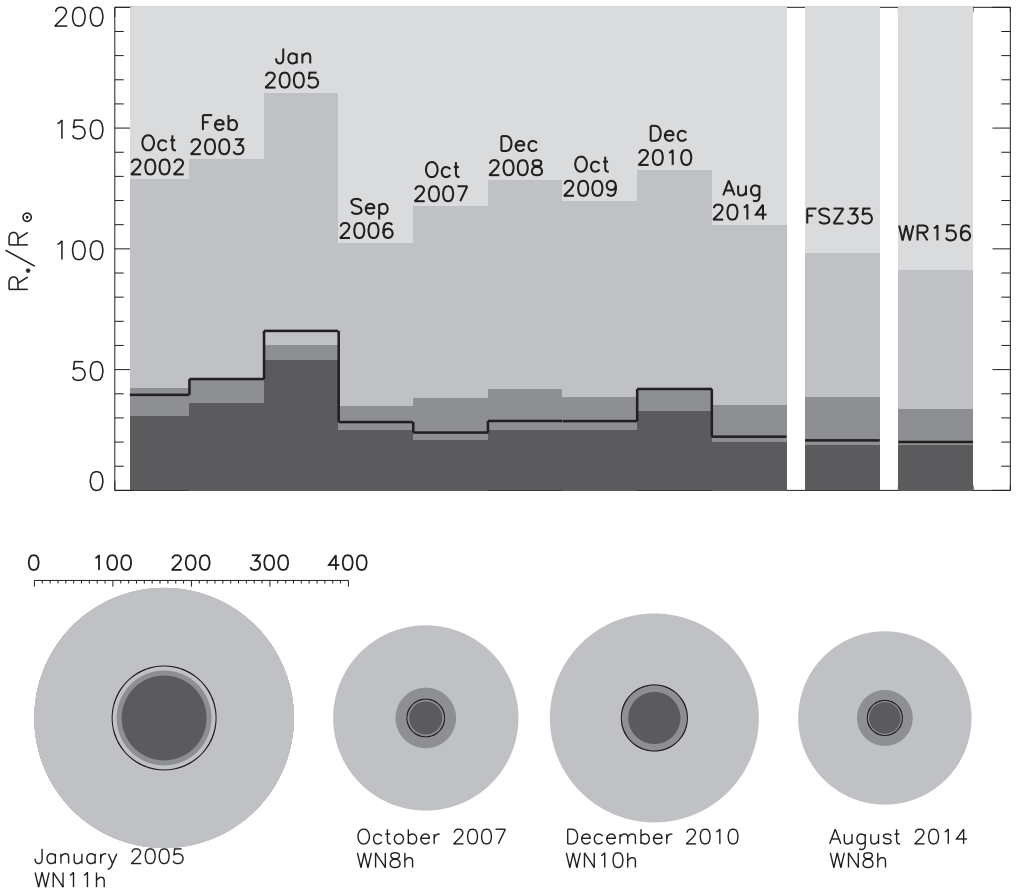

Figure 8. Change of the wind extent with time. Regions with $n_e > 10^{12}$ cm^{-3} are shown in black, $10^{12} > n_e > 10^{11}$ cm^{-3} in dark gray, $10^{11} > n_e > 10^{10}$ cm^{-3} in gray, $10^{10} > n_e$ cm^{-3} in light gray. The solid black line shows the radius where the Rosseland optical depth (τ) is 2/3. WN8h stars FSZ35 and WR156 are also shown for comparison.

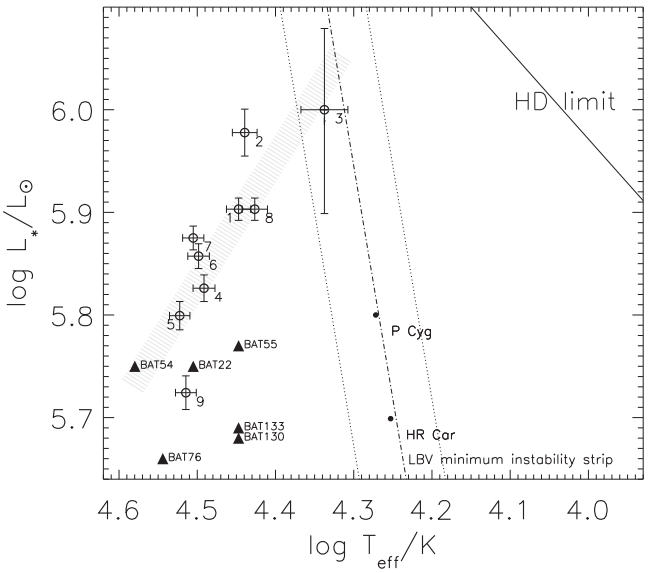

Figure 9. Position of GR 290 in the H–R diagram. The LBV minimum instability strip is traced with a dashed–dotted line, the Humphreys–Davidson limit (Humphreys & Davidson 1994) is shown with a solid line. Dates refer to the point number in the figure: 1 = 2002 October 1, 2 = 2003 February 2, 3 = 2005 January 3, 4 = 2006 September 4, 5 = 2007 October 5, 6 = 2008 December 6, 7 = 2009 October 7, 8 = 2010 December 8, and 9 = 2014 August 9. Also the LBV stars P Cygni and HR Car are shown with circles. Data for these objects were taken from Najarro (2001) and Groh et al. (2009a). Triangles mark late-WN stars taken from Hainich et al. (2014). The hatched strip shows the region crossed by GR 290 during its recent luminosity cycles.

5.2. GR 290 and the WNL Stars

A point to be considered is the present high temperature of GR 290 and its spectrum at minimum, which is very similar to that of WN8h stars. Figure 9 shows that the luminosity and temperature of GR 290 fit well that of late-WN stars. The mass-loss rate of GR 290 is also similar, but the wind velocity of GR 290, $v_\infty = 400$ km s^{-1}, is significantly lower than that of WN8h stars (see Maryeva & Abolmasov 2012a, 2012b). Also the hydrogen abundance of the envelope appears higher than in WNL stars. Figure 10 shows the diagram of the hydrogen mass fraction as a function of luminosity for different evolutionary tracks. GR 290 lies higher than WN8h stars. These results give evidence that, from the evolutionary and structural point of view, GR 290 is younger than WN8h stars.

5.3. Evolutionary Considerations

According to the above derived bolometric luminosity ($\log L_*/L_\odot = 5.8$–5.9) and effective temperature of 22–33 kK, the position of GR 290 fits the 60 $M_\odot$ evolutionary tracks of Chieffi & Limongi (2013) with and without rotation, just to the left of the low temperature loop in the H–R diagram. The Geneva evolutionary tracks for non-rotating models suggest a similar initial mass (see, e.g., Groh et al. 2013). Although all of these tracks were computed for solar metallicity, the initial mass of GR 290 cannot be too far from this value. According to the evolutionary models of Chieffi & Limongi (2013) GR 290 should now be 4 Myr old and have a

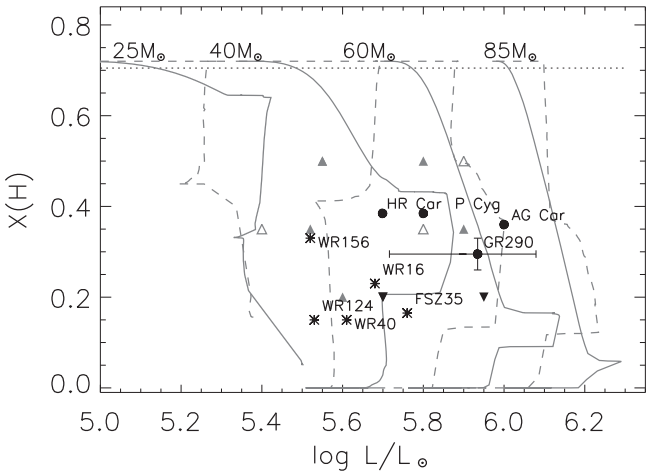

Figure 10. Hydrogen mass fraction as a function of luminosity. Continuous lines show the Geneva tracks for non-rotating models. The position of the LBV and WN stars is also marked. Late WN stars in M31 are shown by triangles, data taken from Sander et al. (2014). WN9 stars are represented with open triangles, WN8 with filled triangles, and WN7 with upturned triangles.

mass of 26 $M_{\odot}$. The star is thus in the mass range where theoretical evolutionary models foresee that, after the O phase and before the Hydrogen-poor Wolf–Rayet (WR) star phase, stars transit from an Of/WN (or WN 9-11) through the LBV phase to a WNL phase. Groh et al. (2014) computed the spectral evolution of a non-rotating 60 $M_{\odot}$ star, that could be appropriate to the case of GR 290. They found that the star first evolves to the right part of the H–R diagram through the hot LBV phase (near the end of core H-burning) to the cool LBV loop of the evolutionary track. Then, after the beginning of core He burning, the star leaves the LBV phase and evolves to early WN, rapidly crossing in a few thousand years the late-WN phase. In the Groh et al. framework, the effective temperature and spectral type of GR 290 would clearly place the star in the WNL phase. The post-LBV phase is further supported by the helium and nitrogen abundances derived in Section 4, which are higher than in the classical LBVs. One should also note that, according to Groh et al. (2014), the lifetime of a 60 $M_{\odot}$ star in the LBV phase is 50 times longer than that in the post-LBV WNL phase, hence we should expect WNL stars to be very rare. The question is whether, in the post-LBV phase, stars still undergo large luminosity variation such as those observed in GR 290.

5.4. Luminosity Variation

As discussed in Section 4, a distinguishing peculiarity of GR 290 is the variation of its bolometric luminosity during its recent apparent luminosity cycles. The evolution of LBVs during the S Dor cycles seems to occur in most cases roughly at constant bolometric luminosity (see, e.g., Smith et al. 1994; de Koter et al. 1996; Walborn et al. 2008). Indeed, the variation of the bolometric luminosity is a point so far observed only in a few LBV cases: Groh et al. (2009b) have found that the bolometric luminosity of AG Car has decreased by a factor of 1.5 from minimum toward the light maximum of the S Dor cycle. A reduction of the bolometric luminosity during the cycle was also derived by Lamers (1995) for S Dor itself. Lamers (1995) interpreted this result in terms of the radiative power being partially transformed into mechanical power in order to expand the outer layers of the star from minimum to maximum. The same explanation was given by Groh et al. (2009b) in the case of AG Car and by Andriesse et al. (1978) to explain the one magnitude decrease of the bolometric luminosity of η Car after the 1843 giant outburst. In the case of GR 290, the power associated to its mass-loss rate is by far too low to explain its changes in bolometric luminosity. In addition, contrary to the cases discussed above, the $L_{\rm bol}$ increases of GR 290 are recorded during its visual luminosity maxima. If, as for instance suggested by Lovekin & Guzik (2014), the GR 290 active phase were triggered by bursts of nuclear energy, an associated increase in bolometric luminosity could occur at the light maxima as observed, due to the energy release associated with these nuclear runaway events. Since changes of the bolometric luminosity of such an amplitude have not been recorded so far in any LBVs, we may argue that the higher temperature of GR 290 plays an important role in the above suggested process.

6. CONCLUSIONS

In summary, we have shown the following.

1. During the last 100 years, GR 290 experienced two phases: one long lasting quasi-stationary, presumably hot phase. Then an active phase started in the mid-20th century with five luminosity maxima separated by 7–10 years.
2. The amplitude of the last variability cycles is decreasing with an associated increase of the stellar temperature at minimum. During this period of time, the stellar temperature is modulated in anti-correlation with the visual luminosity.
3. The star is in all phases much hotter than the other LBVs, reaching an effective temperature of 33 kK at the apparent luminosity minima.
4. During the last two variability cycles, the bolometric luminosity changed following the variation of visual luminosity, being a factor of 1.5 higher at maximum.
5. The bolometric luminosity of GR 290 fits the evolutionary tracks of a $\simeq$ 60 $M\odot$ star. The high effective temperature and WNL-type spectrum place the star after the low temperature loop of the evolutionary tracks, which is thought to be occupied by the LBV stars.
6. At present, the representative point of GR 290 in the H–R diagram is close to that of WN8h stars, but the chemical abundances suggest that the star is younger than them.

The above discussed points lead us to conclude that GR 290 is presently in a short, and thus very rare, transition phase between the LBV evolutionary phase and the nitrogen rich W-R stellar class, as also suggested by Polcaro et al. (2011) and Humphreys et al. (2014).

GR 290, though it is no longer near the LBV minimum instability strip, still might be subject to structural instabilities similar to those which gave rise to the last observed large variability cycles.

We cannot foresee how long these instabilities will last. Following Lovekin & Guzik (2014; Guzik & Lovekin 2014), the instability is due to the hydrogen mixing in the core generating a burst of nuclear energy: presently, such repeated nuclear events should be the extra-energy input to increase the bolometric luminosity of GR 290 during its last outbursts. They will end when the hydrogen percentage in the envelope will become too low to be mixed in the core. However, the steady

decreasing amplitude of the last cycles and gradual increasing of the temperature of GR 290 both suggest that this instability phase will not last too long. This point will require new theoretical studies on the internal instabilities in luminous stars and GR 290 could probably be an ideal target to study this process.

This research has made use of the plate archives of the following astronomical observatories: Asiago, Hamburg, Heidelberg, Yerkes, Pulkovo, SAO. We thank P. Dalle Ave for having performed the scans of the Asiago plates. The plate digitization project of Hamburg Observatory (D. Groote) was funded by DFG grant GR969/4-1. We thank the Istituto Astrofisico de Canarias (IAC) for the use of the 80 cm telescope during the 2012 and 2013 campaigns. We are grateful to Franco Montagni for providing us with his photometric observations of GR 290 at Greve and to the ARA team who helped with the photometric monitoring of the star. The observations at the 6 m BTA telescope were carried out with the financial support of the Ministry of Education and Science of the Russian Federation (agreement No. 14.619.21.0004, project ID RFMEFI61914X0004). O.M. acknowledges the grant of Dynasty Foundation and the Russian Foundation for Basic Research (projects no. 14-02-31247,14-02-00291). This research has made use of the SIMBAD database, operated at CDS, Strasbourg, France. We thank our referee R. Humphreys for providing helpful suggestions to improve the clarity of the paper.

APPENDIX

The Hamburg plates have four different types of Agfa emulsions and no filters. All plates were digitized in transparency mode at the Hamburg Observatory with Epson Expression 10000 XL scannners, at 2400 dpi step, giving a scale of 0.74 arcsec/pixel, in the framework of a legacy project (P.I. D. Groote). Given the fast telescope focal ratio, the images are substantially affected by coma but the region around GR 290 is fairly usable for aperture photometry. We transformed the plate transparency into pseudo-intensity with the formula $I = (U - B)/(T - B)$, where T is the transparency of a given pixel, U is the average transparency of the unexposed plate, and B is the transparency in the center of saturated stars (Nesci et al. 2005). Then we performed aperture photometry on GR 290 with IRAF/apphot, using as the calibration the brightest reference stars of the sequence given in Viotti et al. (2006; namely, from ku-a to ku-h), in the range $B = 14.8$–19.08. We adopted the B magnitude scale, as it is more similar to that of the old plate emulsions. Further stars of the sequence were not usable due to crowding or because they are too faint. The adopted aperture radius was 4 pixels (3 arcsec), comparable to the FWHM of the stars. For each plate, a linear fit between instrumental and nominal magnitudes was derived and found quite satisfactory, with a slope near to the ideal case of 1.00; from these fits we derived the magnitude of GR 290 together with the rms deviation of the comparison stars from the calibration and the slope of the linear fit. To estimate the photometric accuracy of our magnitudes, we also measured a field star of comparable magnitude and used its deviation from the fit as a photometric error, which resulted to be about 0.2 mag.

The Heidelberg plates were digitized with the Heidelberg Nexscan F4100, with a resolution from 100 to 200 pixels per millimeter. The plates found in the Pulkovo archive have been digitized with a Canon 5D MarkII camera. The Yerkes plates were scanned with an EPSON 10000XL at 2400 dpi.

All the POSS plates and the Asiago blue plates (103aO emulsion + GG13 filter) showed calibration curves fully compatible with a linear relation between instrumental and reference magnitudes; the Asiago V plates (103aD emulsion + GG14 filter) instead showed a marked curvature, requiring a parabolic fit. We therefore added a further star in the comparison sequence, fainter than GR 290, in order not to extrapolate its magnitude. The only suitable star in the Viotti et al. (2007) sequence is M31a-262 with $V = 17.61$.

REFERENCES

Andriesse, C. D., Donn, B. D., & Viotti, R. 1978, MNRAS, 185, 771
Calabresi, M., Rossi, C., Gualandi, R., et al. 2014, ATel, 5846
Chieffi, A., & Limongi, M. 2013, ApJ, 764, 1
Clark, J. S., Castro, N., Garcia, M., et al. 2012, A&A, 541, A146
Crowther, P. A., & Smith, L. J. 1997, A&A, 320, 500
de Koter, A., Lamers, H. J. G. L. M., & Schmutz, W. 1996, A&A, 306, 501
Fabrika, S., Sholukhova, O., Becker, T., et al. 2005, A&A, 437, 217
Galleti, S., Bellazzini, M., & Ferraro, F. R. 2004, A&A, 423, 925
Groh, J. H., Damineli, A., Hillier, D. J., et al. 2009a, ApJL, 705, L25
Groh, J. H., Hillier, D. J., Damineli, A., et al. 2009b, ApJ, 698, 1698
Groh, J. H., Meynet, G., Ekström, S., & Georgy, C. 2014, A&A, 564, 30
Groh, J. H., Meynet, G., Georgy, C., & Ekström, S. 2013, A&A, 558, 131
Guzik, C. C., & Lovekin, J. A. 2014, IAUS, 301, 449
Hainich, R., Rühling, U., Todt, H., et al. 2014, A&A, 565, A27
Hillier, D. J., & Miller, D. L. 1998, ApJ, 496, 407
Hippelein, H., Haas, M., Tuffs, R. J., et al. 2003, A&A, 407, 137
Humphreys, R. M., & Davidson, K. 1994, PASP, 106, 1025
Humphreys, R. M., Weis, K., Davidson, K., et al. 2014, ApJ, 790, 48
Kiseleva, T. P., & Khrutskaya, E. V. 2007, SoSyR, 41, 72
Kurtev, R., Sholukhova, O., Borissova, J., & Georgiev, L. 2001, RMxAA, 37, 57
Lamers, H. J. G. L. M. 1995, in ASP Conf. Ser. 83, Astrophysical Applications of Stellar Pulsation, IAU Colloquium 155, ed. R. S. Stobie, & P. A. Whitelock (San Francisco, CA: ASP), 155
Lovekin, J. A., & Guzik, C. C. 2014, MNRAS, 445, 1766
Magrini, L., Stanghellini, L., Corbelli, E., et al. 2010, A&A, 512, A63
Maryeva, O., & Abolmasov, P. 2010, RMxAA, 46, 279
Maryeva, O., & Abolmasov, P. 2012a, MNRAS, 419, 1455
Maryeva, O., & Abolmasov, P. 2012b, MNRAS, 421, 1189
Maryeva, O. V., Afanasiev, V. L., & Panchuk, V. E. 2013, NewA, 25, 2
Massey, P., McNeill, R. T., Olsen, K. A. G., et al. 2007, ApJ, 134, 2474
Morris, P. W., Brownsberge, r. K. R., Conti, P. S., et al. 1993, ApJ, 412, 324
Najarro, F. 2001, in ASP Conf. Ser. 233, P Cygni 2000: 400 years of progress, ed. M. de Groot, & C. Sterken (San Francisco, CA: ASP), 133
Nesci, R., Massaro, E., Rossi, C., et al. 2005, AJ, 130, 1466
Polcaro, V. F., Rossi, C., Viotti, R. F., et al. 2011, AJ, 141, 18
Romano, G. 1978a, IBVS, 1433
Romano, G. 1978b, A&A, 67, 291
Sander, A., Todt, H., Hainich, R., & Hamann, W.-R. 2014, A&A, 563, 89
Schlegel, D. J., Finkbeiner, D. P., & Davies, M. 1998, ApJ, 500, 525
Sholukhova, O. N., Fabrika, S. N., Vlasyuk, V. V., & Burenkov, A. N. 1997, AstL, 23, 458
Sholukhova, O. N., Fabrika, S. N., Zharova, A. V., Valeev, A. F., & Goranskij, V. P. 2011, AstBu, 66, 123
Smith, L. J., Crowther, P. A., & Prinja, R. K. . 1994, A&A, 281, 833
Sterken, C., Sthal, O., Wolf, B., Szeifert, Th., & Lones, A. 1995, A&A, 303, 766
Szeifert, T. 1996, in Liege International Astrophysical Coll. 33, Wolf-Rayet stars in the framework of stellar evolution, 459
van Genderen, A. M. 2001, A&A, 366, 508
Viotti, R. F., Galleti, S., Gualandi, R., et al. 2007, A&A, 464, L53
Viotti, R. F., Rossi, C., Polcaro, V. F., et al. 2006, A&A, 458, 225
Walborn, N. R., Stahl, O., Gamen, R. C., et al. 2008, ApJL, 683, L33
Wolf, B. 1989, A&A, 217, 87